NaV1.5 Na+ channels allosterically regulate the NHE-1 exchanger and promote the activity of breast cancer cell invadopodia

L. Brisson, V. Driffort, L. Benoist, M. Poët, L. Counillon, E. Antelmi, R. Rubino, P. Besson, F. Labbal, S. Chevalier, et al.

$Na_V1.5$ Na^+ channels allosterically regulate the NHE-1 exchanger and promote the activity of breast cancer cell invadopodia

Lucie Brisson[1], Virginie Driffort[1,*], Lauriane Benoist[1,*], Mallorie Poet[2], Laurent Counillon[2], Ester Antelmi[3], Rosa Rubino[3], Pierre Besson[1], Fabien Labbal[2], Stéphan Chevalier[1], Stephan J. Reshkin[3,‡], Jacques Gore[1] and Sébastien Roger[1,4,‡]

[1]Inserm U1069, Nutrition, Croissance et Cancer, Université François-Rabelais de Tours, 10 Boulevard Tonnellé, 37032 Tours, France
[2]CNRS FRE3472, Université de Nice-Sophia Antipolis, Faculté des Sciences Parc Valrose – 06108 Nice, France
[3]Department of Biosciences, Biotechnology and Pharmacological Sciences, University of Bari, Via Amendola 165A, I-70126 Bari, Italy
[4]UFR Sciences et Techniques, Département de Physiologie Animale, Université François-Rabelais de Tours, Parc de Grandmont, 37200 Tours, France

*These authors contributed equally to this work
‡Authors for correspondence (stephanjoel.reshkin@uniba.it; sebastien.roger@univ-tours.fr)

Accepted 10 July 2013
Journal of Cell Science 126, 4835–4842

doi: 10.1242/jcs.123901

Summary

The degradation of the extracellular matrix by cancer cells represents an essential step in metastatic progression and this is performed by cancer cell structures called invadopodia. $Na_V1.5$ (also known as SCN5A) Na^+ channels are overexpressed in breast cancer tumours and are associated with metastatic occurrence. It has been previously shown that $Na_V1.5$ activity enhances breast cancer cell invasiveness through perimembrane acidification and subsequent degradation of the extracellular matrix by cysteine cathepsins. Here, we show that $Na_V1.5$ colocalises with Na^+/H^+ exchanger type 1 (NHE-1) and caveolin-1 at the sites of matrix remodelling in invadopodia of MDA-MB-231 breast cancer cells. NHE-1, $Na_V1.5$ and caveolin-1 co-immunoprecipitated, which indicates a close association between these proteins. We found that the expression of $Na_V1.5$ was responsible for the allosteric modulation of NHE-1, rendering it more active at the intracellular pH range of 6.4–7; thus, it potentially extrudes more protons into the extracellular space. Furthermore, $Na_V1.5$ expression increased Src kinase activity and the phosphorylation (Y421) of the actin-nucleation-promoting factor cortactin, modified F-actin polymerisation and promoted the acquisition of an invasive morphology in these cells. Taken together, our study suggests that $Na_V1.5$ is a central regulator of invadopodia formation and activity in breast cancer cells.

Key words: Voltage-gated Na^+ channels, SCN5A, Na^+/H^+ exchanger type 1, Caveolae, Invadopodia, Cancer cell invasiveness

Introduction

Breast cancer is the primary cause of death by cancer in women worldwide, and patients mostly die because of metastases. At the cellular level, a determining step in the development of metastases depends on the capacity of cancer cells to degrade and migrate through the extracellular matrix (ECM). This is performed by invadopodia, which are actin-rich organelles that protrude into the ECM and are responsible for its proteolysis through the recruitment of both membrane-associated and extracellularly released soluble proteases (Linder et al., 2011). The proteolytic activity of invadopodia is highly dependent on the acidification of the peri-invadopodial extracellular compartment (Brisson et al., 2012) through the localised activity of Na^+/H^+ exchanger type 1 (NHE-1) (Busco et al., 2010; Magalhaes et al., 2011). Voltage-gated Na^+ channels (Na_V) are abnormally expressed in cancer cells from different epithelial origins (e.g. breast, lung, prostate, colon and cervix) and, in melanoma, their function might be associated with cancer progression (Diaz et al., 2007; Hernandez-Plata et al., 2012; House et al., 2010; Roger et al., 2006; Roger et al., 2007; Yildirim et al., 2012). The $Na_V1.5$ isoform (also known as SCN5A) is overexpressed in breast cancer tissues, is associated with the development of metastases and is functional in highly invasive breast cancer cells (Fraser et al., 2005; Roger et al., 2003; Yang et al., 2012). In the highly aggressive human MDA-MB-231 breast cancer cell line, the activity of $Na_V1.5$ enhances ECM degradation by increasing the activity of acidic cysteine cathepsins through the acidification of the pericellular microenvironment (Brisson et al., 2011; Gillet et al., 2009). In the present study, we demonstrate that $Na_V1.5$ interacts with NHE-1 in focal ECM degradation sites corresponding to caveolin-1-containing invadopodia. We also found that $Na_V1.5$ activity controls Src kinase activity, cortactin phosphorylation, actin cytoskeletal dynamics and is responsible for the allosteric modulation of NHE-1, thus enhancing invadopodial proteolytic activity.

Results and Discussion

Invadopodia are key structures involved in matrix remodelling by cancer cells (Linder, 2007). Therefore, we analysed the ability of MDA-MB-231 cells to degrade ECM by growing them on a planar matrix of Matrigel™ containing DQ-gelatin, a fluorogenic substrate for proteases. Multiple subcellular areas of degradation were observed, which we designate ‘focal areas’; these

colocalised with F-actin condensations (Fig. 1A). High-resolution structured-illumination microscopy (SIM) imaging of these areas showed intense spots of matrix degradation. Approximately 10% of the studied spots were surrounded by F-actin rings, forming structures of ~2 μm in diameter in axial (*xy*) sections (Fig. 1B,C). These structures can also be seen on sagittal (*xz*) and coronal (*yz*) projections. They were located below the cell body and showed a substantial penetration into the ECM (>5 μm depth) (Fig. 1B; supplementary material Fig. S1A). This F-actin organisation might correlate with that observed in electron microscopy studies in the same cancer cells (Schoumacher et al., 2010) and with the protrusive structure of podosomes observed in dendritic cells (Gawden-Bone et al., 2010). One hypothesis that is consistent with these observations is that some invadopodia show a particular structure, namely that the protrusions into the ECM have a hollow tubular shape, with the centre showing the strongest proteolytic activity. Such a structure would allow a tight control of pH and protease activity inside the invadopodium. Alternatively, these images could be interpreted as being the endocytosed degradation products inside the invadopodium.

We used a MagicRed® [MR-$(RR)_2$] substrate assay to determine the activity of the extracellular protease cathepsin B in the MDA-MB-231 cells growing on DQ-gelatin, and found that the focal areas of DQ-gelatin degradation in the Matrigel™ had an intense activity of cathepsin B (Pearson's coefficient, r=0.65, Fig. 1D). This is consistent with our previous study suggesting that cathepsin B had a substantial role in the invasion of MDA-MB-231 cells (Gillet et al., 2009). Moreover, there was a strong colocalisation between $Na_V1.5$ channels and cathepsin B (r=0.82, supplementary material Fig. S1B). $Na_V1.5$ also colocalised with MT1-MMP (also known as MMP14), which has been proposed to serve as a good invadopodia marker (Linder et al., 2011) (r=0.69, Fig. 2A). We have previously shown that $Na_V1.5$ is located in caveolin-1-rich membrane fractions (caveolae) (Brisson et al., 2011). Using immunofluorescence imaging, we found a punctate labelling of $Na_V1.5$ that was highly correlated with caveolin-1 (r=0.75, Fig. 2B). Caveolae are dynamic lipid raft platforms at the plasmalemma that allow protein clustering, and it is thought that they are important for the composition and functioning of invadopodia (Caldieri et al., 2009; Yamaguchi et al., 2009) given that they could recruit multiple components required for the focal degradation of the ECM (Caldieri and Buccione, 2010; Caldieri et al., 2012; Yamaguchi and Oikawa, 2010). Here, we observed that caveolin-1 strongly colocalised with F-actin condensation loci (r=0.75, Fig. 2C). Proximity ligation assays indicated that there was a close association of $Na_V1.5$ and caveolin-1 in areas of DQ-gelatin degradation (Fig. 2D). Fig. 2E shows that invadopodial fractions from MDA-MB-231 cells, obtained as previously described (Busco et al., 2010) and characterised by the presence of the invadopodia markers cortactin, focal adhesion kinase (FAK) and MT1-MMP, contained NHE-1 as well as caveolin-1, $Na_V1.5$, and immature and mature forms of cathepsin B, which is the key protease in $Na_V1.5$-dependent ECM invasion (Gillet et al., 2009). Using SIM technology, we found that $Na_V1.5$ and NHE-1 were strongly colocalised (r=0.92) in restricted domains protruding into the extracellular matrix (Fig. 3A; supplementary material Fig. S1C). Because the SIM apparatus is only equipped with two lasers, we assessed the

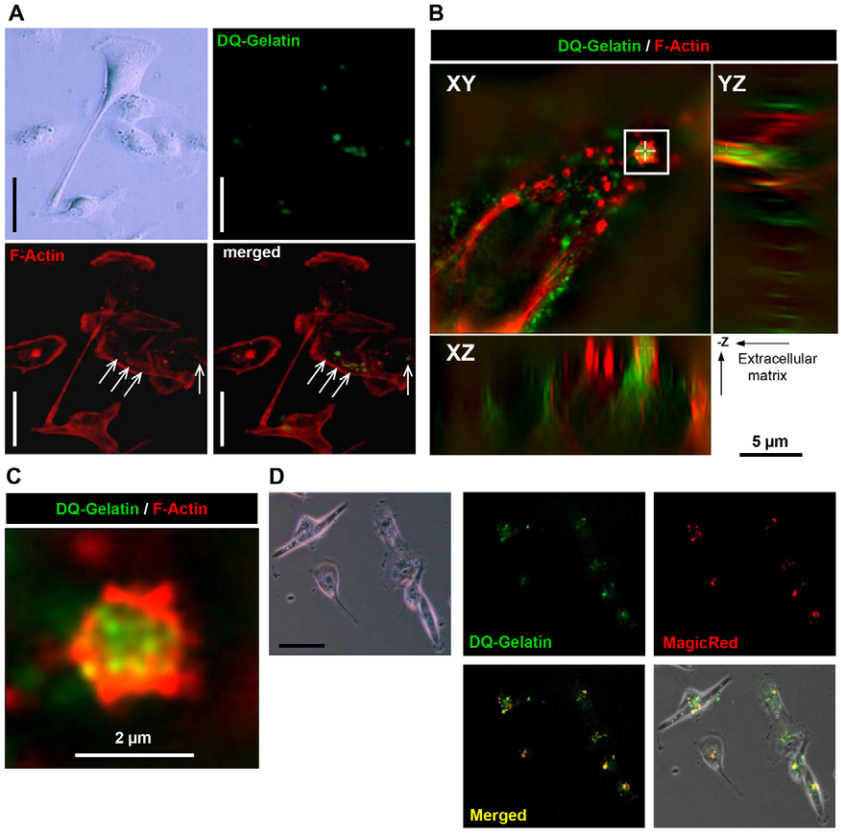

Fig. 1. Characterisation of invadopodia of MDA-MB-231 breast cancer cells. Cells were grown for 24 hours on a planar matrix of Matrigel™ containing DQ-Gelatin®. (A) F-actin staining with phalloidin–Alexa594 (red) showing high-density sub-cellular structures (white arrows). Cleaved DQ-gelatin® was detected in 'focused' areas under the cancer cells (green), close to F-actin condensations (merged). Scale bars: 50 μm. (B,C) SIM imaging of invadopodia defined as being dense F-actin circular structures (red) colocalised with *in situ* matrix degradation (green). (B) Invadopodium in an axial plan (XY) with a proteolytic spot (green) surrounded by F-actin structures (boxed region). YZ and XZ projections from the selected area (white cross) show the insertion of this protrusive structure into the ECM. (C) Enlargement of the invadopodial section selected in B. (D) Fluorescence imaging showing the colocalisation of proteolytic spots (green) with cathepsin B activity in the extracellular matrix [MagicRed™ substrate, MR-(RR)2, red staining]. Scale bar: 30 μm.

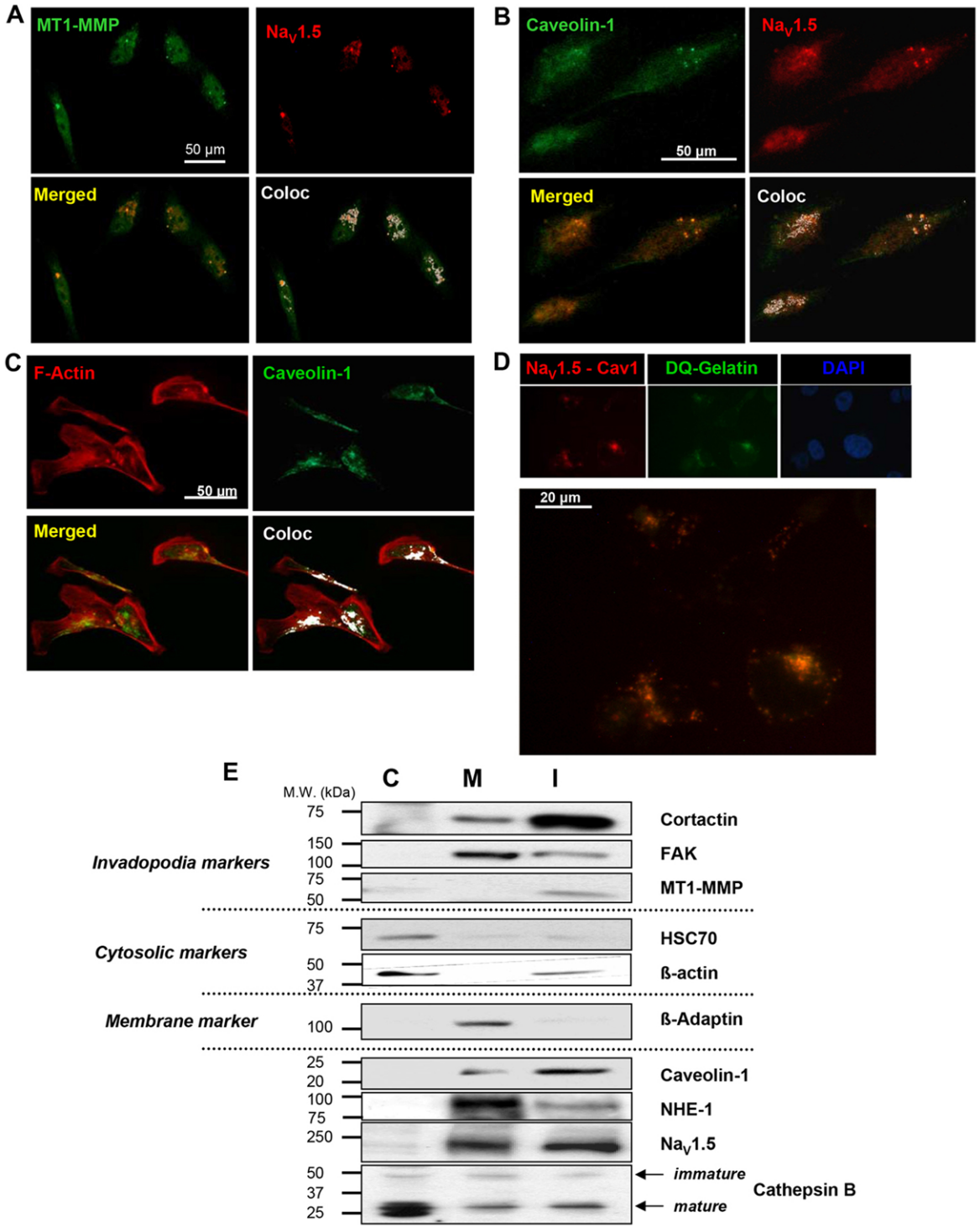

Fig. 2. $Na_V1.5$ colocalises with caveolin-1 in invadopodia of MDA-MB-231 breast cancer cells. (A–C) Immunofluorescence imaging performed on MDA-MB-231 breast cancer cells grown on Matrigel™ and showing focal areas of strong colocalisation (Coloc, white pixels) between (A) MT1-MMP (green) and $Na_V1.5$ (red), (B) caveolin-1 (green) and $Na_V1.5$ (red), and (C) spots of F-actin (phalloidin–Alexa594, red) and caveolin-1 (green). (D) *In situ* proximity ligation assays (DUOLINK In cell coIP) showing a strong proximity between $Na_V1.5$ and caveolin-1 (red dots) in areas of matrix degradation (green). (E) Invadopodia (I) entrapped into a 2% gelatin matrix were fractionated and separated from cytosol (C)- and membrane (M)-enriched fractions. The quality of the fractions was assessed using invadopodia (cortactin, FAK, MT1-MMP), cytosolic (HSC70, β-actin) and membrane (β-adaptin) markers.

colocalisation of $Na_V1.5$ and/or NHE-1 with ECM degradation spots in invadopodia by using confocal imaging of cells seeded on a layer of Matrigel™ containing BSA-BODIPY-FL. This showed that there were multiple protruding organelles involved in matrix proteolysis at the underside of the cell body, which strongly colocalised with NHE-1 and $Na_V1.5$ (Fig. 3B, supplementary

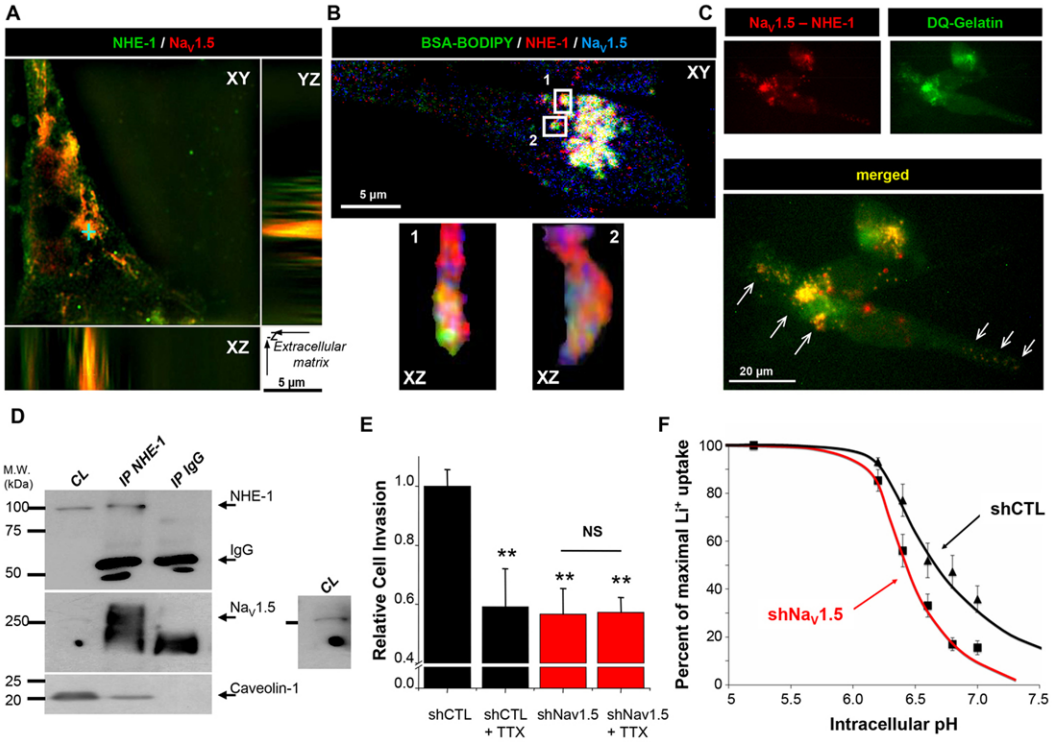

Fig. 3. $Na_V1.5$ interacts with, and allosterically modulates NHE-1 function. (A) SIM immunofluorescence imaging of NHE-1 (green) and $Na_V1.5$ (red) performed on a MDA-MB-231 breast cancer cell grown on Matrigel™ and showing spots of strong colocalisation (XY) corresponding to structures protruding into the ECM, as observed with XZ and YZ projections from the selected area (blue cross). (B) Confocal imaging of NHE-1 (red) and $Na_V1.5$ (blue) from a cell cultured on BSA-BODIPY-FL-containing matrix, which releases green fluorescence when degraded. Numerous focal zones of degradation were identified in axial sections (XY), which showed colocalisation with NHE-1 and $Na_V1.5$. Two areas (1 and 2) were selected and analyzed in sagittal sections (XZ) demonstrating a strong colocalisation of NHE-1 and $Na_V1.5$ and showed protrusive structure in the areas of matrix degradation. (C) Proximity ligation assays from MDA-MB-231 cells grown on Matrigel™ and showing spots of strong colocalisation (red spots) between $Na_V1.5$ and NHE-1 almost completely limited (see arrows) to areas of focal digestion (green). (D) NHE-1 was detected in total cell lysates (CL) and was immunoprecipitated (IP NHE-1) with an anti-NHE-1 antibody. Anti-immunoglobulin was used as a negative control to rule out non-specific binding in the immunoprecipitation (IP IgG). On the right, is an image that was obtained with a longer exposure time to enable the detection of $Na_V1.5$ in CL. (E) Relative matrix invasion by shCTL and $shNa_V1.5$ MDA-MB-231 cells in presence or absence of TTX (30 µM) (n=4). **P<0.01 compared with siCTL; NS, not significant. (F) Initial rates of the NHE-1 exchanger measured using the fast kinetics of Li^+ uptake. Dose–response curves for the NHE-1 activity in the $shNa_V1.5$ (squares) and shCTL (triangles) cells at different intracellular pH values are shown.

material Fig. S1D). Proximity ligation assays also confirmed the close vicinity of NHE-1 and $Na_V1.5$ in focused matrix degradation spots (Fig. 3C). As can be seen in Fig. 3D, both $Na_V1.5$ and caveolin-1 coimmunoprecipitated with NHE-1, consistent with a (direct or indirect) interaction between these three membrane proteins. By contrast, $Na_V1.5$ and caveolin-1 were not immunodetected when a control IgG was used for precipitation.

NHE-1 is ubiquitously expressed at the plasma membrane of all mammalian cells, has a very low activity at the physiological intracellular pH (pHi) and activates rapidly when the cytoplasm becomes acidic, following a dimeric Monod–Wyman–Changeux cooperative mechanism (Lacroix et al., 2004). We next decided to investigate whether the presence of $Na_V1.5$ in breast cancer cells could modify the sensitivity of NHE-1 to internal protons. To do so, we constructed two stable cell lines derived from MDA-MB-231 cells: one expressing a shRNA targeting the expression of the *SCN5A* ($shNa_V1.5$) and another one expressing a shRNA that does not target any known gene (shCTL). $ShNa_V1.5$ reduced the mRNA expression of *SCN5A* gene by ~80%, which resulted in the complete disappearance of Na^+ currents in these cells (supplementary material Fig. S2A–C). Treating shCTL cells with 30 µM tetrodotoxin (TTX) to block Na^+ currents reduced the relative invasion by ~40% (Fig. 3E) without affecting cell viability (supplementary material Fig. S3C) or proliferation (Gillet et al., 2009). $ShNa_V1.5$ cells had a ~40% reduced invasion compared to shCTL cells, and TTX had no supplementary effect. We then measured NHE-1 activity as a function of pHi, by measuring the fast kinetics of Li^+ uptake, and showed that the presence of active $Na_V1.5$ channels in MDA-MB-231 cancer cells significantly (P<0.05) increased Li^+ uptake in pHi range 6.4 to 7 (Fig. 3F; supplementary material Fig. S2D). The change in cooperativity strongly suggests that $Na_V1.5$ function in cancer cells allosterically increases NHE-1 activity in neutral ranges of pHi.

MDA-MB-231 cancer cells display a ‘fibroblast-like’ shape when grown on a planar layer of Matrigel™, exhibiting a rich F-actin labelling in the barbed-end of the lamellipodial leading edge, as well as at the rear of the cell. This shape, characteristic of highly invasive cells, was lost when cells did not express $Na_V1.5$ channels or were treated with TTX (Fig. 4A,B). In these two cases the F-actin cytoskeleton was disturbed, showed uniform submembrane localisation and was associated with a change in cell morphology characterised by the increase of the

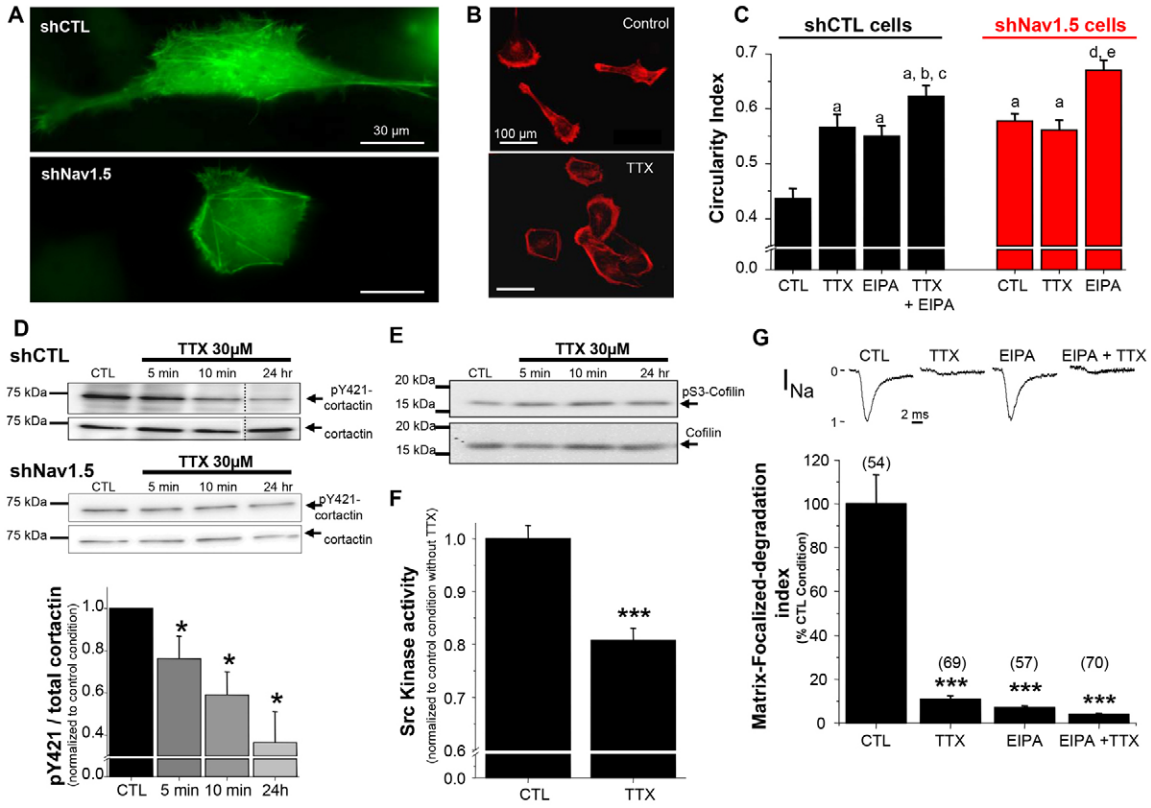

Fig. 4. $Na_V1.5$ controls F-actin cytoskeleton, cell morphology and foci of matrix degradation in MDA-MB-231 cancer cells. (A) shCTL and sh$Na_V1.5$ cells were transfected with LifeAct–GFP to visualize the striking differences in F-actin cytoskeleton and cell morphology between both MDA-MB-231-derived cell types. (B) Representative photographs of shCTL cells cultured on a Matrigel™ treated with vehicle (control) or 30 µM TTX. The F-actin cytoskeleton was stained with phalloidin–Alexa594. (C) Experiments described in B were performed in either shCTL and sh$Na_V1.5$ cancer cells that were either untreated (CTL) or treated with TTX (30 µM), or EIPA (1 µM) or a combination of TTX + EIPA. A cell circularity index was calculated using ImageJ© software for each the cell type and different treatment (n=45–208 cells analysed). Statistically different at P<0.001: a, from shCTL, CTL condition; b, from shCTL, TTX condition; c, from shCTL, EIPA condition; d, from sh$Na_V1.5$, CTL condition; e, from sh$Na_V1.5$, TTX condition. (D) Upper panel, blots showing pY421-cortactin and total cortactin in non-treated (CTL) or 5 minutes, 10 minutes or 24 hours with 30 µM TTX-treated shCTL cells. Same experiments were performed in sh$Na_V1.5$ cancer cells. Lower panel, a quantification of pY241 relative to total cortactin (normalised to the control condition) from shCTL cells (n=5). *P<0.05. (E) Blots showing pS3-cofilin and total cofilin levels in shCTL cells treated for 5 minutes, 10 minutes or 24 hours with 30 µM TTX or non-treated (CTL) (n=3). (F) Src kinase activity was assessed from total shCTL cell lysates after a 10-minute long treatment with 30 µM TTX or with a control solution (CTL, vehicle), and the activity was normalised to the control condition. ***P<0.001. (G) MDA-MB-231 cells were cultured on Matrigel™ containing DQ-Gelatin®. Invadopodial activities were assessed from untreated cells (CTL) or from cells treated with 30 µM TTX or 1 µM EIPA or a combination of TTX plus EIPA. A 'Matrix-Focalised-degradation activity index' was calculated, as indicated in supplementary material Fig. S4, for each treatment. ***P<0.001. Representative Na^+ currents (I_{Na}) in each treatment, normalised to the maximal current recorded in the control condition, recorded for a depolarisation from −100 to −5 mV, are shown above the graph.

circularity index of cancer cells (Fig. 4C). The actin-nucleation-promoting factor cortactin (encoded by the gene *CTTN*) is a crucial regulator of the actin cytoskeletal dynamics and, consequently, of the formation and function of invadopodia. Cortactin is known to bind (through a SH3 domain) and to activate the Arp2/3 complex, which is responsible for the formation of branched F-actin and the enhancement of cell migration (MacGrath and Koleske, 2012). Cortactin also binds and inhibits the actin-severing protein cofilin (encoded by the gene *CFL1*). The phosphorylation of cortactin releases cofilin and leads to the increase of polymerizing actin barbed ends (Oser et al., 2009). By performing prognostic analyses of gene expression in cohorts of breast cancer patients (bc-GenExMiner v3.0; http://bcgenex.centregauducheau.fr; Jézéquel et al., 2012) we found that the overexpression of both *CTTN* [P<0.0001; hazard ratio (a measure of survival in patients with the condition compared with that of those without), 1.49, 95% confidence interval, 1.26–1.70] and *CFL1* (P<0.0001; hazard ratio 1.40, 95% confidence interval, 1.19–1.64) genes were associated with a reduced survival without metastatic relapse (supplementary material Fig. S3A,B) indicating the crucial role of these proteins in cancer cell invasion and the development of metastases. Here, we found that inhibiting NHE-1 by the use of ethyl-isopropyl amiloride (EIPA) also increased cell circularity in both shCTL and sh$Na_V1.5$ cells (Fig. 4C). This could be because the activity of cofilin is pH dependent, and, hence, the intracellular alkalinisation induced by NHE-1 activity might disrupt the interaction between cofilin and cortactin thus enhancing the initiation of actin polymerisation (Frantz et al., 2008; Pope et al., 2004). However, there are partially additive effects on cell circularity when combining both TTX and EIPA as compared with the use of one of these two inhibitors separately. We

hypothesise that, independently of its regulation of NHE-1 activity, $Na_V1.5$ could modulate F-actin polymerisation and invadopodia formation. Cortactin can also be released from cofilin when phosphorylated on tyrosine residues (Y421 and Y466) by Src kinase, which regulates its ability to promote branched actin nucleation by modulating its ability to recruit binding partners (Oser et al., 2010; Oser et al., 2009). We found that inhibiting the activity of $Na_V1.5$ channels with TTX, which had no effect on cell viability (supplementary material Fig. S3C), rapidly reduced the level of pY421-cortactin [by 26.4±8.7% after 5 minutes, 36.0±9.8% after 10 minutes and by 48.5±16.2% after 24 hours] (Fig. 4D). This was not due to a general dephosphorylation mechanism (supplementary material Fig. S3D–F) and was not observed in cells that did not express $Na_V1.5$ ($shNa_V1.5$). An analysis of the levels of pY421-cortactin at various time points of the TTX treatment, revealed that there were reductions in the amount of pY421-cortactin at all time points analyzed (5, 10, 20 and 30 minutes, and 1, 2 and 24 hours of treatment) compared to the control conditions (data not shown). By contrast, blocking $Na_V1.5$ had no effect on the phosphorylation of cofilin on S3 (Fig. 4E), which has been shown to be critical for binding to actin (Arber et al., 1998). This suggests that $Na_V1.5$ might regulate Src kinase and not LIM kinase. Indeed, we found that TTX induced a reduction in Src kinase activity (Fig. 4F). As a result, a reduction of both invadopodia formation and activity was expected upon inhibition $Na_V1.5$. The number of pixels corresponding to the colocalisation of F-actin condensation areas and focal spots of DQ-gelatin proteolysis were quantified per cell, giving a 'matrix-focalised-degradation index' (Fig. 4G; supplementary material Fig. S4). Inhibiting $Na_V1.5$ with TTX, and NHE-1 with EIPA, resulted in 89% and 93% inhibition of the matrix focal degradation, respectively. Combining TTX and EIPA reduced matrix degradation by 96% (Fig. 4G).

Voltage-gated Na^+ channels (Na_V) have long been considered as being characteristic of excitable cells (Catterall, 2012). However, different Na_V isoforms have been found in non-excitable cancer cells and their function enhances cancer cell invasiveness (Roger et al., 2006). In highly invasive breast cancer cells and in high-grade breast cancer biopsies, the overexpression of the $Na_V1.5$ isoform has been associated with ECM remodelling and an increased probability of developing metastases (Gillet et al., 2009; Yang et al., 2012). Indeed, $Na_V1.5$ promotes ECM proteolysis through NHE-1-dependent acidic activation of the extracellular cathepsins B and S (Brisson et al., 2011; Gillet et al., 2009). NHE-1 is already known to have a substantial role in extracellular acidification and in the invasiveness of cancer cells (Bourguignon et al., 2004; Busco et al., 2010; Cardone et al., 2005; Stock and Schwab, 2009), and any signalling pathway increasing its activity could make cancer cells become more aggressive. In this study, we showed for the first time that $Na_V1.5$ interacts with and allosterically increases NHE-1 activity in a range of pHi between 6.4 and 7.0. We propose that these interactions occur in caveolae of the invadopodial compartment and are responsible for an increased ECM degradative activity. Indeed, caveolae are membrane domains that 'build' protein–protein signalling complexes (Harvey and Calaghan, 2012) that are required for both invadopodia formation and ECM degradative activity (Caldieri et al., 2012; Caldieri et al., 2009; Yamaguchi et al., 2009). As such, caveolae could be a signalling platform in invadopodia for Na_V- and NHE-1-dependent cancer cell invasiveness. Because of their invaginated structure, caveolae also provide a space with restricted diffusion for ionic fluxes that could be responsible for local changes in membrane potential and signalling cascades. We also found that $Na_V1.5$ function in cancer cells enhanced Src kinase activity and Y421 cortactin phosphorylation, which could contribute to the acquisition of an aggressive phenotype. Although the mechanism has not yet been elucidated, this could be in line with the observation that membrane depolarisation regulates the actin polymerisation:actin depolymerisation ratio and thus, the F-actin network directly under the plasmalemma (Callies et al., 2011). This effect on actin polymerisation could also be dependent on the interaction of actin with NHE-1 through the association with actin-binding proteins of the ERM (ezrin, radixin and moesin) family (Baumgartner et al., 2004; Cardone et al., 2005).

Na_V channels have also been identified in other invasive cells, such as macrophages (Carrithers et al., 2007) and microglial cells (Black and Waxman, 2012), and blocking their activity has been shown to reduce cell invasiveness. It has also been proposed that this effect depends on the regulation of formation of podosomes (Carrithers et al., 2009).

In conclusion, we have shown that $Na_V1.5$ channels promote the degradative invadopodial activity in breast cancer cells, both by modifying the F-actin cytoskeleton and enhancing the activity of NHE-1. The participation of Na_V channels in the constitution and activity of ECM degrading compartments could be a general feature shared by invasive cancer and non-cancer cells.

Materials and Methods

Inhibitors, chemicals and antibodies

Tetrodotoxin was purchased from Latoxan (France). Fluorescent probes were purchased from Tebu-Bio (France). Other drugs and chemicals were purchased from Sigma-Aldrich (France). Secondary horseradish peroxidase (HRP)-conjugated antibodies were from Santa Cruz Biotechnology.

Cell culture and cell lines

MDA-MB-231 human breast cancer cells were cultured in DMEM supplemented with 5% fetal calf serum (FCS), and grown at 37℃ in a humidified 5% CO_2 incubator.

We constructed a lentiviral vector encoding a short hairpin RNA (shRNA) specifically targeting human *SCN5A* transcripts using the same protocol as previously described (Jelassi et al., 2011). Briefly, the sequence encoding $shNa_V1.5$ was obtained by PCR elongation of two partially complementary primers: 5′-GGATCCCCAAGGCACAAGTGCGTGCGCAATTCAAGAGA-3′ and 5′-AAGCTTAAAAAAAGGCACAAGTGCGTGCGCAATCTCTTGAA-3′. We also constructed a lentiviral vector expressing an untargeted shRNA (pLenti-shCTL), by using the following primers: 5′-GGATCCCCGCCGAC-CAATTCACGGCCGTTCAAGAGACG-3′ and 5′-AAGCTTAAAAAGCCGA-CCAATTCACGGCCGTCTCTTGAACG-3′. These experiments resulted in $shNa_V1.5$ and shCTL cell lines. Cell viability was assessed as previously described (Brisson et al., 2011; Gillet et al., 2009).

Cellular electrophysiology

Patch pipettes were pulled from borosilicate glass to a resistance of 4–6 MΩ. Na^+ currents were recorded, in whole-cell configuration, under voltage-clamp mode using an Axopatch 200B amplifier (Axon Instrument, USA) as previously described (Gillet et al., 2009). The external Na^+ solution was (in mM): NaCl 140, KCl 4, $MgCl_2$ 1, $CaCl_2$ 2, D-glucose 11.1, HEPES 10, adjusted to pH 7.4 with NaOH (1M). The external Li^+ solution used LiCl 140 mM to replace NaCl. Intrapipette solution was (in mM): K-Glutamate 125, KCl 20, $CaCl_2$ 0.37, $MgCl_2$ 1, Mg-ATP 1, EGTA 1, HEPES 10, adjusted to pH 7.2.

In vitro invasion assays

Cell invasiveness was analysed as previously described (Brisson et al., 2011) using culture inserts with an 8-µm pore size filter covered with Matrigel™ (Becton Dickinson, France).

Measurement of initial rates of NHE-1 functioning

Cells seeded on 24-well plates were acidified in Li^+- and Na^+-free solutions containing 2.5 µM nigericin and 140 mM KCl, and were calibrated at various pH values ranging from 5.2 to 7.2 as previously described (Lacroix et al., 2004; Milosavljevic et al., 2010). Measurements were performed after a 3-minute incubation in the uptake medium supplemented with 3 mM LiCl, followed by four rapid rinses in ice-cold PBS. Cells were solubilised in 0.25M nitric acid, and Li^+ was measured using atomic absorption spectrometry (Zeeman furnace system, Thermo Scientific). The initial rates of NHE-1 were calculated as the EIPA (10 µM)-sensitive Li^+ accumulation per well divided by the protein quantity.

Invadopodial fractionation

Invadopodia, embedded into a thick layer of gelatin, were isolated and separated from cytosolic and membrane fractions as previously described (Busco et al., 2010). Primary antibodies used were: mouse anti-NHE1 (Chemicon), mouse anti-HSC70 (Santa-Cruz Biotechnology), rabbit anti-caveolin-1 (Cell Signaling), goat anti-β-adaptin (BD Biosciences), rabbit anti-human $Na_V1.5$ (Sigma-Aldrich), rabbit anti-focal adhesion kinase (FAK, Santa-Cruz Biotechnology) and rabbit anti-human cathepsin B (Fitzgerald).

Coimmunoprecipitations and western blotting

Cells were washed with PBS and lysed in presence of a lysis buffer (50 mM Tris-HCl, pH 7, 100 mM NaCl, 5 mM $MgCl_2$, 10% glycerol, 1 mM EDTA), containing 1% Triton-X-100 and protease inhibitors. Coimmunoprecipitations (co-IP) experiments were performed using Bio-Adembeads PAG magnetic beads (Ademtech, France) according to standard protocols. Two types of lysate–antibody mixes were prepared and incubated overnight at 4℃. Each mix contained 500 µg total cell lysate in 500 µl lysis buffer and 1 µg antibody (mouse anti-NHE1 or mouse control IgG). Cortactin and cofilin were immunodetected using mouse anti-cortactin, rabbit anti-pY421 cortactin, rabbit anti-cofilin and rabbit anti-pS3 cofilin antibodies, respectively (all from Millipore).

Fluorescence imaging

Cells were cultured on Matrigel™ (4 mg/ml)-coated coverslips for 24 hours then washed in PBS, fixed with 3.7% ice-cold paraformaldehyde in PBS. For confocal imaging, cells were permeabilised with 0.1% Triton X-100 and saturated with 0.1% gelatin in PBS. For epifluorescence and SIM imaging, they were permeabilised with a solution containing 50 mM NH_4Cl, 1% BSA and 0.02% saponin, and saturated in 3% BSA and 3% normal goat serum (NGS). Coverslips were incubated with primary antibodies then washed with 0.1% BSA in PBS and incubated with secondary fluorescent-conjugated antibodies. F-actin was stained with phalloidin–Alexa594. Primary antibodies used were anti-human $Na_V1.5$ (Sigma-Aldrich), anti-NHE1 (Abcam 4E9, or Santa-Cruz 4E9), anti-caveolin 1 (Cell Signaling). Fluorescent-conjugated antibodies used were anti-rabbit-Ig–TexasRed, anti-rabbit-Ig–AlexaFluor488, anti-goat-Ig–DyLight488, anti-rabbit-Ig–AlexaFluor350, anti-mouse-Ig–AlexaFluor568 and anti-mouse-Ig–AlexaFluor488. MagicRed substrate [MR-$(RR)_2$,, 1:1000, Immunochemistry Technologies] was used to assess cathepsin B activity. In some experiments, cells were transfected with LifeAct-TagGFP2 plasmids (Ibidi) allowing the visualisation of F-actin dynamics in living cells.

Epifluorescence imaging

Gelatinolytic activity was assessed by culturing cells for 24 hours on a planar Matrigel™ matrix containing 25 µg/ml DQ-Gelatin®. Epifluorescence microscopy was performed with a Nikon TI-S microscope and analysed using both NIS-BR software (Nikon, France) and ImageJ© software 1.38I (http://rsbweb.nih.gov/ij). A circularity index was calculated as $\frac{4\pi \times \text{area}}{\text{perimeter}^2}$. A value approaching 0 indicates an increasingly elongated shape, whereas a value of 1.0 indicates a perfect circle. Pearson's coefficients were calculated with the ImageJ colocalisation plugin.

SIM imaging

SIM experiments were performed at the Nikon Imaging Center at the Institut Curie-CNRS (Paris), using a Nikon Eclipse Ti inverted microscope equipped with a MCL Piezo stage, two lasers (488 nm, 100 mW and 561 nm 100 mW), a 100× CFI Plan Apo TIRF (NA 1.49) oil immersion objective and an EM-CCD Camera iXon DU897 (Andor).

Confocal imaging

Cells were seeded on a layer of Matrigel™ (4 mg/ml) containing a substrate for digestion localisation (BSA-BODIPY-FL, 30 µg/mL) and observed at 600× magnification using a oil immersion objective with a Leica TCS SP5 II AOBS laser scanning confocal microscope equipped with He/Ne-633 and Argon-488 lasers with 495–519 (B2-A) and 642–660 (Cy5) nm excitation filters. Proximity ligation assays were performed according to standard protocols using the Duolink-'In-cell Co-IP' kit (OLink Biosciences) (Söderberg et al., 2006).

Measurements of Src family kinase activity

Src kinase activity was assessed using the ProFluor® Src family kinase assay (Promega, France) according to the manufacturer's instructions. shCTL MDA-MB-231 cells were treated for 10 minutes with 30 µM TTX or with a control solution (CTL, vehicle), then were lysed. Src kinase activities were assessed from total cell lysate samples containing 3 µg total proteins.

Statistical analyses

Data are displayed as mean±s.e.m. (n=sample size). Student's t-tests were used to compare groups showing Gaussian distributions and homogenous variances, alternatively a Mann–Whitney rank sum test was performed. Statistical significance is indicated as: *$P<0.05$; **$P<0.01$ and ***$P<0.001$.

Acknowledgements

We thank I. Domingo and C. Le Roy for technical and administrative assistance, J.-C. Pagès, C. Collin, M.-L. Jourdan and V. Joulin for the development of shRNA and the Nikon Imaging Center at the Institute Curie-CNRS Paris.

Author contributions

L. Brisson, V.D., L. Benoist, M.P., L.C. E.A., R.R., F.L. performed experiments. Experiments were conceived and designed by L. Brisson, L.C., P.B., S.J.R., J.G and S.R. Data were analysed and interpreted by L. Brisson, L.C., P.B., S.C., S.J.R., J.G and S.R. Overall supervision of work was performed by S.J.R., J.G and S.R. The paper was written by S.J.R. and S.R.

Funding

This work was supported by the 'Ministère de la Recherche et des Technologies'; the Inserm; the 'Ligue Nationale Contre le Cancer'; the 'Programme Hubert Curien – Galileo' (Campus France); and the 'Associazione Italiana per la Ricerca sul Cancro' (AIRC) [grant number 11348 to S.J.R.]. The SJR laboratory is part of the Italian network 'Istituto Nazionale Biostrutture e Biosistemi' (INBB), the Centro di Eccellenza di Genomica in Campo Biomedico ed Agrario of the University of Bari and the project BioBoP of the Region Puglia.

Supplementary material available online at
http://jcs.biologists.org/lookup/suppl/doi:10.1242/jcs.123901/-/DC1

References

Arber, S., Barbayannis, F. A., Hanser, H., Schneider, C., Stanyon, C. A., Bernard, O. and Caroni, P. (1998). Regulation of actin dynamics through phosphorylation of cofilin by LIM-kinase. *Nature* **393**, 805-809.

Baumgartner, M., Patel, H. and Barber, D. L. (2004). Na(+)/H(+) exchanger NHE1 as plasma membrane scaffold in the assembly of signaling complexes. *Am. J. Physiol.* **287**, C844-C850.

Black, J. A. and Waxman, S. G. (2012). Sodium channels and microglial function. *Exp. Neurol.* **234**, 302-315.

Bourguignon, L. Y., Singleton, P. A., Diedrich, F., Stern, R. and Gilad, E. (2004). CD44 interaction with Na+-H+ exchanger (NHE1) creates acidic microenvironments leading to hyaluronidase-2 and cathepsin B activation and breast tumor cell invasion. *J. Biol. Chem.* **279**, 26991-27007.

Brisson, L., Gillet, L., Calaghan, S., Besson, P., Le Guennec, J. Y., Roger, S. and Gore, J. (2011). Na(V)1.5 enhances breast cancer cell invasiveness by increasing NHE1-dependent H(+) efflux in caveolae. *Oncogene* **30**, 2070-2076.

Brisson, L., Reshkin, S. J., Goré, J. and Roger, S. (2012). pH regulators in invadosomal functioning: proton delivery for matrix tasting. *Eur. J. Cell Biol.* **91**, 847-860.

Busco, G., Cardone, R. A., Greco, M. R., Bellizzi, A., Colella, M., Antelmi, E., Mancini, M. T., Dell'Aquila, M. E., Casavola, V., Paradiso, A. et al. (2010). NHE1 promotes invadopodial ECM proteolysis through acidification of the peri-invadopodial space. *FASEB J.* **24**, 3903-3915.

Caldieri, G. and Buccione, R. (2010). Aiming for invadopodia: organizing polarized delivery at sites of invasion. *Trends Cell Biol.* **20**, 64-70.

Caldieri, G., Giacchetti, G., Beznoussenko, G., Attanasio, F., Ayala, I. and Buccione, R. (2009). Invadopodia biogenesis is regulated by caveolin-mediated modulation of membrane cholesterol levels. *J. Cell. Mol. Med.* **13 8B**, 1728-1740.

Caldieri, G., Capestrano, M., Bicanova, K., Beznoussenko, G., Baldassarre, M. and Buccione, R. (2012). Polarised apical-like intracellular sorting and trafficking regulates invadopodia formation and degradation of the extracellular matrix in cancer cells. *Eur. J. Cell Biol.* **91**, 961-968.

Callies, C., Fels, J., Liashkovich, I., Kliche, K., Jeggle, P., Kusche-Vihrog, K. and Oberleithner, H. (2011). Membrane potential depolarization decreases the stiffness of vascular endothelial cells. *J. Cell Sci.* **124**, 1936-1942.

Cardone, R. A., Casavola, V. and Reshkin, S. J. (2005). The role of disturbed pH dynamics and the Na+/H+ exchanger in metastasis. *Nat. Rev. Cancer* **5**, 786-795.

Carrithers, M. D., Dib-Hajj, S., Carrithers, L. M., Tokmoulina, G., Pypaert, M., Jonas, E. A. and Waxman, S. G. (2007). Expression of the voltage-gated sodium channel NaV1.5 in the macrophage late endosome regulates endosomal acidification. *J. Immunol.* **178**, 7822-7832.

Carrithers, M. D., Chatterjee, G., Carrithers, L. M., Offoha, R., Iheagwara, U., Rahner, C., Graham, M. and Waxman, S. G. (2009). Regulation of podosome formation in macrophages by a splice variant of the sodium channel SCN8A. *J. Biol. Chem.* **284**, 8114-8126.

Catterall, W. A. (2012). Voltage-gated sodium channels at 60: structure, function and pathophysiology. *J. Physiol.* **590**, 2577-2589.

Diaz, D., Delgadillo, D. M., Hernández-Gallegos, E., Ramírez-Domínguez, M. E., Hinojosa, L. M., Ortiz, C. S., Berumen, J., Camacho, J. and Gomora, J. C. (2007). Functional expression of voltage-gated sodium channels in primary cultures of human cervical cancer. *J. Cell. Physiol.* **210**, 469-478.

Frantz, C., Barreiro, G., Dominguez, L., Chen, X., Eddy, R., Condeelis, J., Kelly, M. J., Jacobson, M. P. and Barber, D. L. (2008). Cofilin is a pH sensor for actin free barbed end formation: role of phosphoinositide binding. *J. Cell Biol.* **183**, 865-879.

Fraser, S. P., Diss, J. K., Chioni, A. M., Mycielska, M. E., Pan, H., Yamaci, R. F., Pani, F., Siwy, Z., Krasowska, M., Grzywna, Z. et al. (2005). Voltage-gated sodium channel expression and potentiation of human breast cancer metastasis. *Clin. Cancer Res.* **11**, 5381-5389.

Gawden-Bone, C., Zhou, Z., King, E., Prescott, A., Watts, C. and Lucocq, J. (2010). Dendritic cell podosomes are protrusive and invade the extracellular matrix using metalloproteinase MMP-14. *J. Cell Sci.* **123**, 1427-1437.

Gillet, L., Roger, S., Besson, P., Lecaille, F., Gore, J., Bougnoux, P., Lalmanach, G. and Le Guennec, J. Y. (2009). Voltage-gated Sodium Channel Activity Promotes Cysteine Cathepsin-dependent Invasiveness and Colony Growth of Human Cancer Cells. *J. Biol. Chem.* **284**, 8680-8691.

Harvey, R. D. and Calaghan, S. C. (2012). Caveolae create local signalling domains through their distinct protein content, lipid profile and morphology. *J. Mol. Cell. Cardiol.* **52**, 366-375.

Hernandez-Plata, E., Ortiz, C. S., Marquina-Castillo, B., Medina-Martinez, I., Alfaro, A., Berumen, J., Rivera, M. and Gomora, J. C. (2012). Overexpression of NaV 1.6 channels is associated with the invasion capacity of human cervical cancer. *Int. J. Cancer* **130**, 2013-2023.

House, C. D., Vaske, C. J., Schwartz, A. M., Obias, V., Frank, B., Luu, T., Sarvazyan, N., Irby, R., Strausberg, R. L., Hales, T. G. et al. (2010). Voltage-gated Na+ channel SCN5A is a key regulator of a gene transcriptional network that controls colon cancer invasion. *Cancer Res.* **70**, 6957-6967.

Jelassi, B., Chantôme, A., Alcaraz-Pérez, F., Baroja-Mazo, A., Cayuela, M. L., Pelegrin, P., Surprenant, A. and Roger, S. (2011). P2X(7) receptor activation enhances SK3 channels- and cystein cathepsin-dependent cancer cells invasiveness. *Oncogene* **30**, 2108-2122.

Jézéquel, P., Campone, M., Gouraud, W., Guérin-Charbonnel, C., Leux, C., Ricolleau, G. and Campion, L. (2012). bc-GenExMiner: an easy-to-use online platform for gene prognostic analyses in breast cancer. *Breast Cancer Res. Treat.* **131**, 765-775.

Lacroix, J., Poët, M., Maehrel, C. and Counillon, L. (2004). A mechanism for the activation of the Na/H exchanger NHE-1 by cytoplasmic acidification and mitogens. *EMBO Rep.* **5**, 91-96.

Linder, S. (2007). The matrix corroded: podosomes and invadopodia in extracellular matrix degradation. *Trends Cell Biol.* **17**, 107-117.

Linder, S., Wiesner, C. and Himmel, M. (2011). Degrading devices: invadosomes in proteolytic cell invasion. *Annu. Rev. Cell Dev. Biol.* **27**, 185-211.

MacGrath, S. M. and Koleske, A. J. (2012). Cortactin in cell migration and cancer at a glance. *J. Cell Sci.* **125**, 1621-1626.

Magalhaes, M. A., Larson, D. R., Mader, C. C., Bravo-Cordero, J. J., Gil-Henn, H., Oser, M., Chen, X., Koleske, A. J. and Condeelis, J. (2011). Cortactin phosphorylation regulates cell invasion through a pH-dependent pathway. *J. Cell Biol.* **195**, 903-920.

Milosavljevic, N., Duranton, C., Djerbi, N., Puech, P. H., Gounon, P., Lagadic-Gossmann, D., Dimanche-Boitrel, M. T., Rauch, C., Tauc, M., Counillon, L. et al. (2010). Nongenomic effects of cisplatin: acute inhibition of mechanosensitive transporters and channels without actin remodeling. *Cancer Res.* **70**, 7514-7522.

Oser, M., Yamaguchi, H., Mader, C. C., Bravo-Cordero, J. J., Arias, M., Chen, X., Desmarais, V., van Rheenen, J., Koleske, A. J. and Condeelis, J. (2009). Cortactin regulates cofilin and N-WASp activities to control the stages of invadopodium assembly and maturation. *J. Cell Biol.* **186**, 571-587.

Oser, M., Mader, C. C., Gil-Henn, H., Magalhaes, M., Bravo-Cordero, J. J., Koleske, A. J. and Condeelis, J. (2010). Specific tyrosine phosphorylation sites on cortactin regulate Nck1-dependent actin polymerization in invadopodia. *J. Cell Sci.* **123**, 3662-3673.

Pope, B. J., Zierler-Gould, K. M., Kühne, R., Weeds, A. G. and Ball, L. J. (2004). Solution structure of human cofilin: actin binding, pH sensitivity, and relationship to actin-depolymerizing factor. *J. Biol. Chem.* **279**, 4840-4848.

Roger, S., Besson, P. and Le Guennec, J. Y. (2003). Involvement of a novel fast inward sodium current in the invasion capacity of a breast cancer cell line. *Biochim. Biophys. Acta* **1616**, 107-111.

Roger, S., Potier, M., Vandier, C., Besson, P. and Le Guennec, J. Y. (2006). Voltage-gated sodium channels: new targets in cancer therapy? *Curr. Pharm. Des.* **12**, 3681-3695.

Roger, S., Rollin, J., Barascu, A., Besson, P., Raynal, P. I., Iochmann, S., Lei, M., Bougnoux, P., Gruel, Y. and Le Guennec, J. Y. (2007). Voltage-gated sodium channels potentiate the invasive capacities of human non-small-cell lung cancer cell lines. *Int. J. Biochem. Cell Biol.* **39**, 774-786.

Schoumacher, M., Goldman, R. D., Louvard, D. and Vignjevic, D. M. (2010). Actin, microtubules, and vimentin intermediate filaments cooperate for elongation of invadopodia. *J. Cell Biol.* **189**, 541-556.

Söderberg, O., Gullberg, M., Jarvius, M., Ridderstråle, K., Leuchowius, K. J., Jarvius, J., Wester, K., Hydbring, P., Bahram, F., Larsson, L. G. et al. (2006). Direct observation of individual endogenous protein complexes in situ by proximity ligation. *Nat. Methods* **3**, 995-1000.

Stock, C. and Schwab, A. (2009). Protons make tumor cells move like clockwork. *Pflugers Arch.* **458**, 981-992.

Yamaguchi, H. and Oikawa, T. (2010). Membrane lipids in invadopodia and podosomes: key structures for cancer invasion and metastasis. *Oncotarget* **1**, 320-328.

Yamaguchi, H., Takeo, Y., Yoshida, S., Kouchi, Z., Nakamura, Y. and Fukami, K. (2009). Lipid rafts and caveolin-1 are required for invadopodia formation and extracellular matrix degradation by human breast cancer cells. *Cancer Res.* **69**, 8594-8602.

Yang, M., Kozminski, D. J., Wold, L. A., Modak, R., Calhoun, J. D., Isom, L. L. and Brackenbury, W. J. (2012). Therapeutic potential for phenytoin: targeting Na(v)1.5 sodium channels to reduce migration and invasion in metastatic breast cancer. *Breast Cancer Res. Treat.* **134**, 603-615.

Yildirim, S., Altun, S., Gumushan, H., Patel, A. and Djamgoz, M. B. (2012). Voltage-gated sodium channel activity promotes prostate cancer metastasis in vivo. *Cancer Lett.* **323**, 58-61.

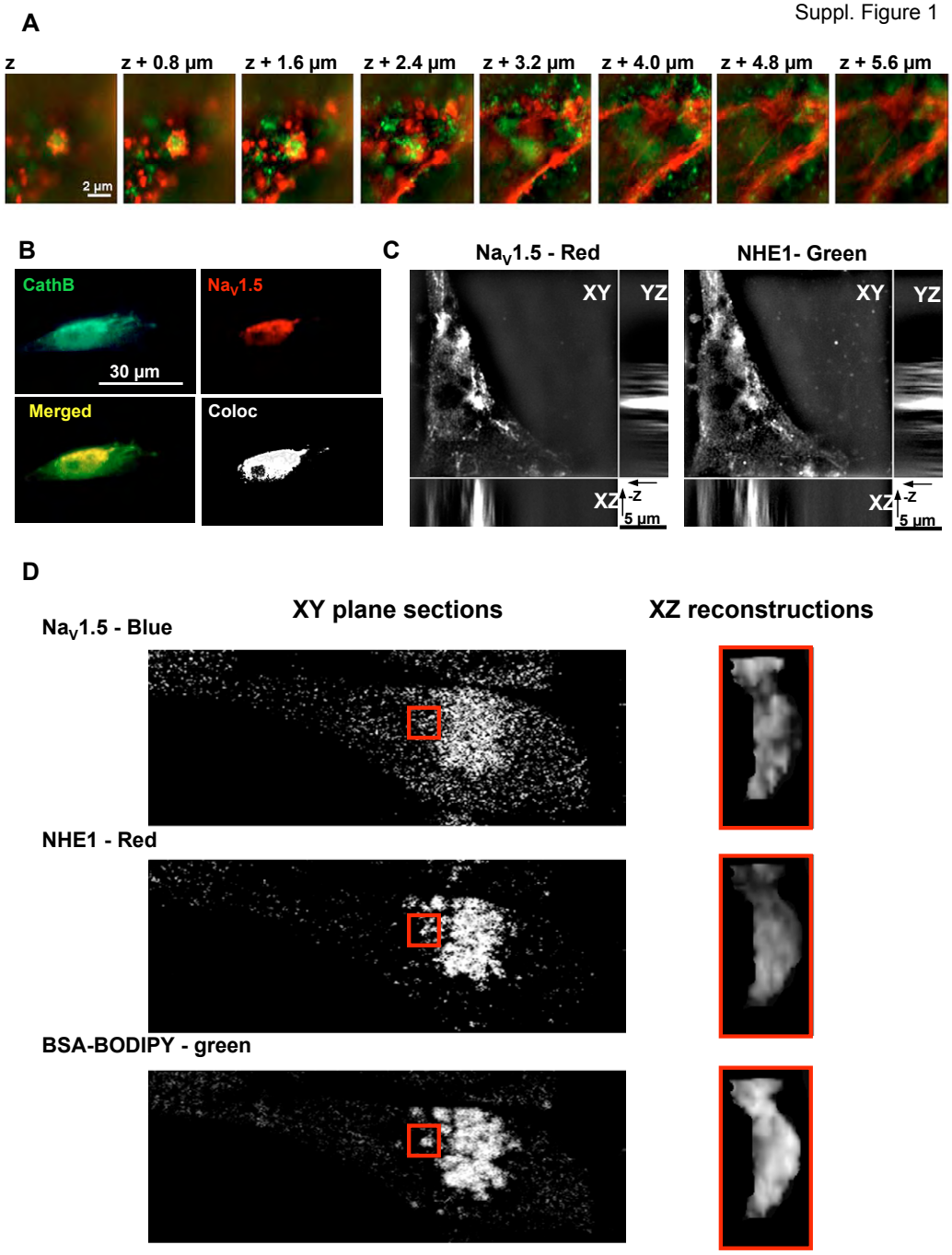

Fig. S1. A, Cells were grown for 24 h on a planar matrix of Matrigel™ containing DQ-Gelatin®. SIM imaging of invadopodia defined as being dense F-actin circular structures (red) co-localized with *in situ* matrix degradation (green). YZ and XZ projections from the selected area (white cross) show the insertion of this protrusive structure into the ECM. This figure represents Z-stage representations of XY plane sections taken from the ECM side (-Z) to the cell body. The 8 images shown are separated by 0.8 µm in the Z-dimension away from the matrix towards the cell. The invadopodium identified in an axial plan (XY) in figure 1B and showing a proteolytic spot (green) surrounded by F-actin structures is located below the cell body and is profoundly penetrating the ECM (> 5 µm depth). **B,** Representative photographs of immunofluorescent stainings performed on a MDA-MB-231 cancer cell grown on a Matrigel™-composed extracellular matrix and showing a strong co-localization between the protease Cathepsin B (CathB, green) and Na$_V$1.5 channels (red) (Pearsons'r= 0.82). Since cells were permeabilized in order to immunodetect Na$_V$1.5 channels, we can not discriminate between extracellular and intracellular cathepsins. However, as shown in figure 1E there is a strong cathepsin B activity in the extracellular milieu suggesting that these proteases could be addressed and released closely to membrane areas containing Na$_V$1.5 channels. **C**, Split channels from Structured-Illumination Microscopy immunofluorescence experiments imaging showed in Figure 3A showing NHE-1 (green) and Na$_V$1.5 (red) labelling performed on a MDA-MB-231 breast cancer cell grown on Matrigel™ and showing spots of strong co-localization (XY) corresponding to protrusive structures into the ECM. **D,** Split channels from confocal immunofluorescence experiments imaging showed in Figure 3B showing NHE-1 (green) and Na$_V$1.5 (Blue) labelling performed on a MDA-MB-231 breast cancer cell grown on Matrigel™ and showing spots of strong co-localization in areas of matrix degradation (green) in a XY plane section. One area is selected (red rectangle) and is presented in a XZ projection, corresponding to protrusive structures into the ECM.

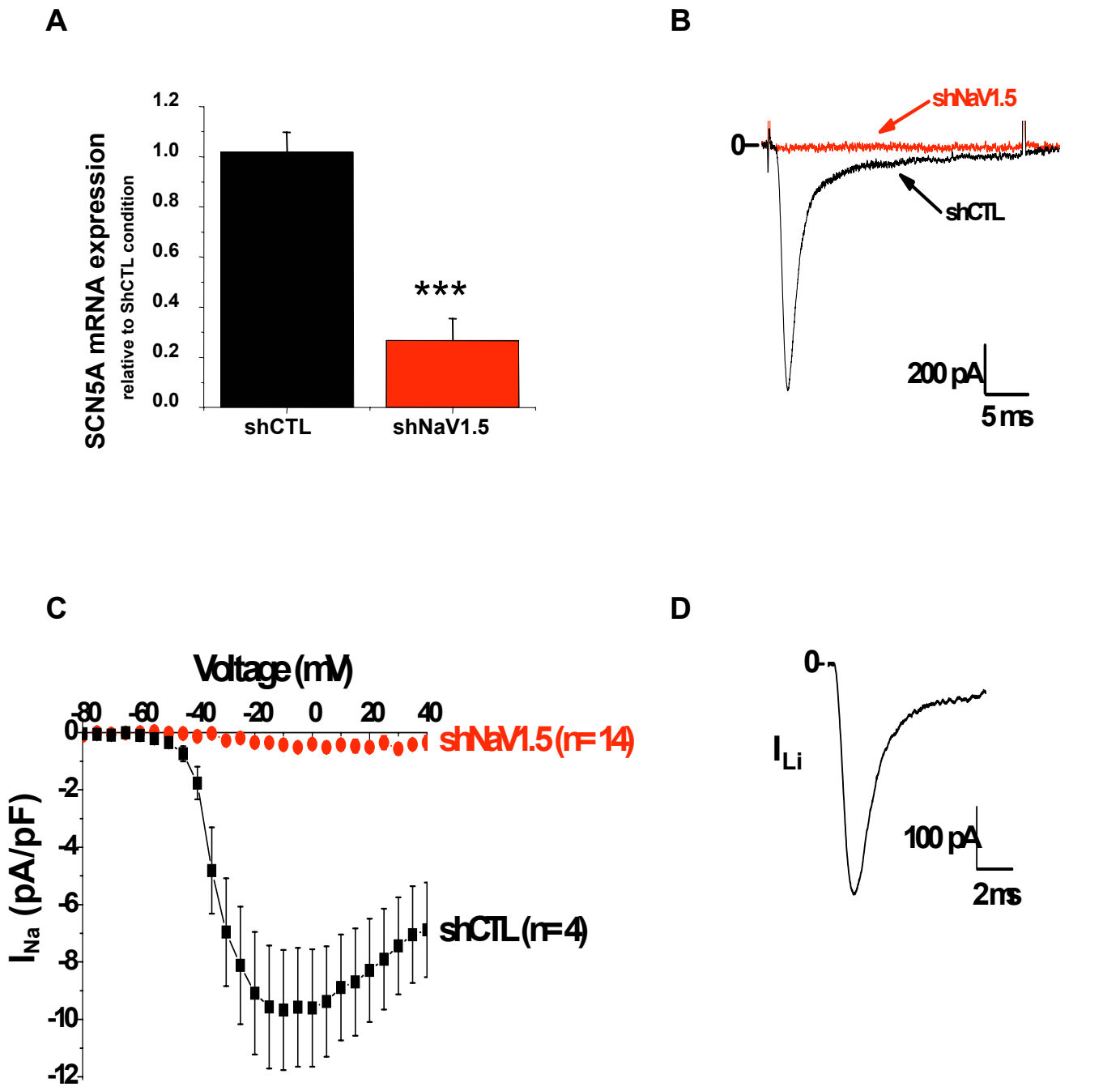

Fig. S2. Lentiviral transduction of wild-type MDA-MB-231 cells generated two stable cell lines: one expressing a shRNA targeting the expression of the *SCN5A* gene transcript (shNa$_V$1.5), and one control cell line expressing a shRNA not targeting any known gene (shCTL). **A**, The efficacy of transduction was assessed by RT-qPCR on Na$_V$1.5 gene expression (n= 6 separate experiments, $p<0.001$). **B**, Representative sodium current (I_{Na}) recorded for a depolarisation from -100 to -5 mV in shCTL and non-existent I_{Na} in shNa$_V$1.5 cells. **C**, Mean ± SEM I_{Na} current-voltage relationships constructed from 4 shCTL and 14 shNa$_V$1.5 cells. **D,** Representative inward currents recorded for a depolarisation from -100 to -5 mV in one MDA-MB-231 shCTL cell in the lithium-containing external solution thus corresponding to a Li^+ current (I_{Li}).

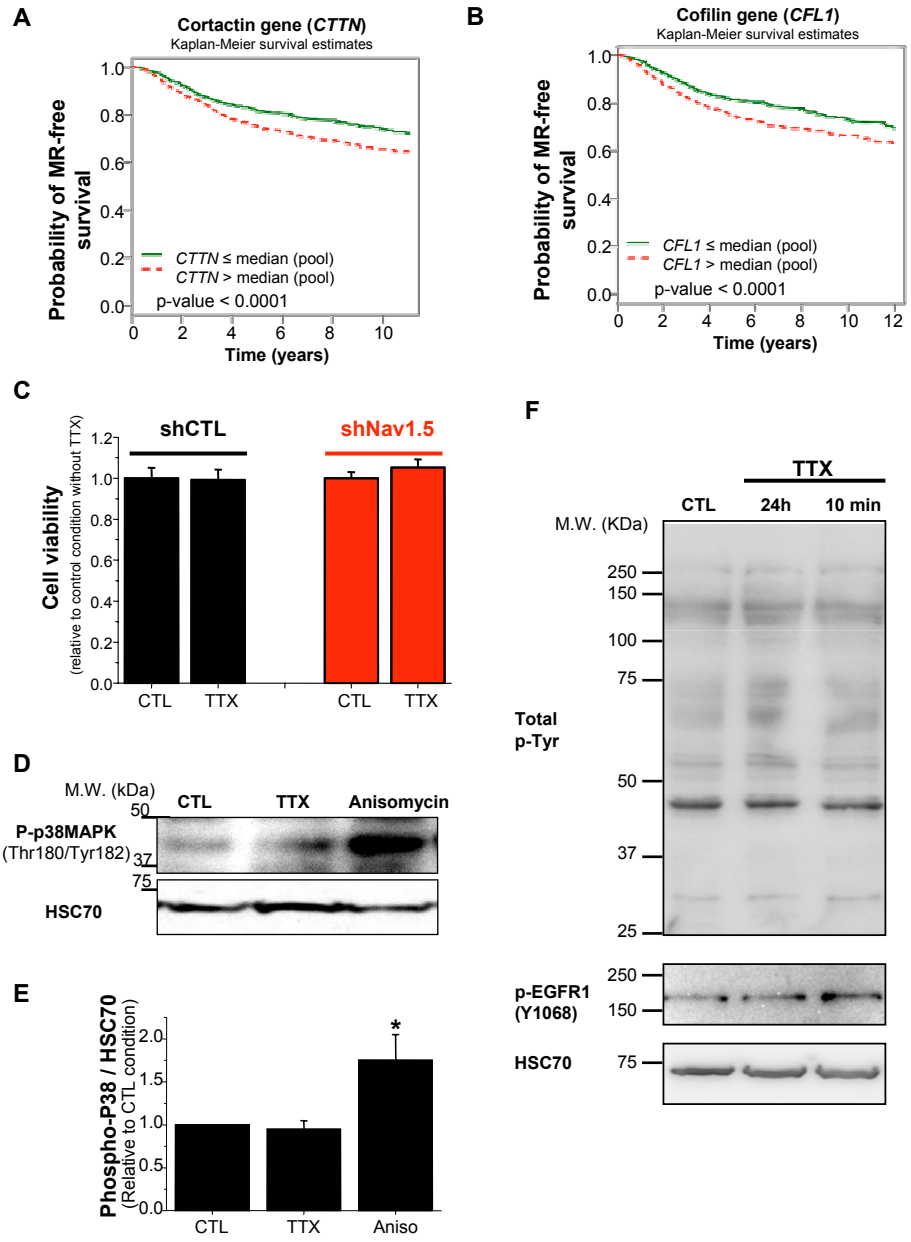

Fig. S3: A *and B,* Prognostic analyses of gene expression in breast cancers - were performed using the software ***Breast Cancer Gene-Expression Miner*** (bc-GenExMiner v3.0; http://bcgenex.centregauducheau.fr) developed by the Integrated Center of Oncology René Gauducheau (Nantes-Saint Herblain, France), based on DNA microarrays results collected from published cohorts. Statistical tests were conducted on each of the individual cohorts and on pooled cohorts as described (Jezequel et al., 2012). Kaplan-Meier metastatic-relapse (MR)-free survival analyses were performed on data pooled from cohorts (see Methods) for the expression of **A**, cortactin (gene *CTTN,* n= 2566 patients) and **B**, cofilin (gene *CFL1,* n= 2314 patients). Cox results are displayed on the curve. **C**, In order to assess the cell survival, shCTL and shNa$_V$1.5 cancer cells were seeded at 1.5 x 10^4 cells per well in 24 well-plates in their respective culture medium in absence (CTL) or in presence of 30 µM TTX (TTX). The cells were cultured for 24 hours and the quantities of living cells were determined using the tetrazolium salt assay as previously described (Gillet et al., 2009). The cell viability was expressed as formazan absorbance at 570 nm and expressed as a percentage of the control condition in the absence of TTX. Results were validated by manual cell counting. Three independent experiments were performed. Results were normalized to the control condition of each cell line and indicate that the TTX treatment, at the maximal duration used to assess cancer cell morphology and cortactin phosphorylation (Y421), had no effect on cell viability. **D-E**, MDA-MB-231 cancer cells were cultured for 24h in absence (CTL, vehicle) or in presence of 30 µM TTX (TTX) or 10 nM anisomycin (Aniso) and the phosphorylation of p38 MAPK on Thr180/Tyr182 was analysed by western blot experiments using a mouse anti-Phospho Thr180/Tyr182 p38MAPK antibody (Cell Signalling, 1/1,000). HSC-70 was immunodetected using a primary mouse anti-HSC70 antibody (Santa Cruz Biotechnology, 1/30,000). **D,** Representative western blot experiment showing that TTX (30 µM) did not modify the level of phosphorylated p38 while anisomycin, known to strongly activate the stress-induced MAP kinases p38, increased it. **E**, Diagram showing the quantification of P-p38MAPK, normalized to HSC-70, in the treatment conditions used in D. N = 3 independent experiments. *, $p<0.05$ as compared to CTL or to TTX condition. There is no statistical difference between CTL and TTX conditions. **E,** Representative western blot experiments showing that TTX (30 µM) applied for 10 min or 24 hr did not modify the level of total phospho-tyrosine (Mouse Anti-Phospho-Tyrosine, Millipore, 4G10, 1/1,000), nor the level of phospho-EGFR1 (Y1068, mouse antibody, Cell Signaling, 1H12, 1/2,000). Therefore, TTX is not responsible for a general mechanism of dephosphorylation.

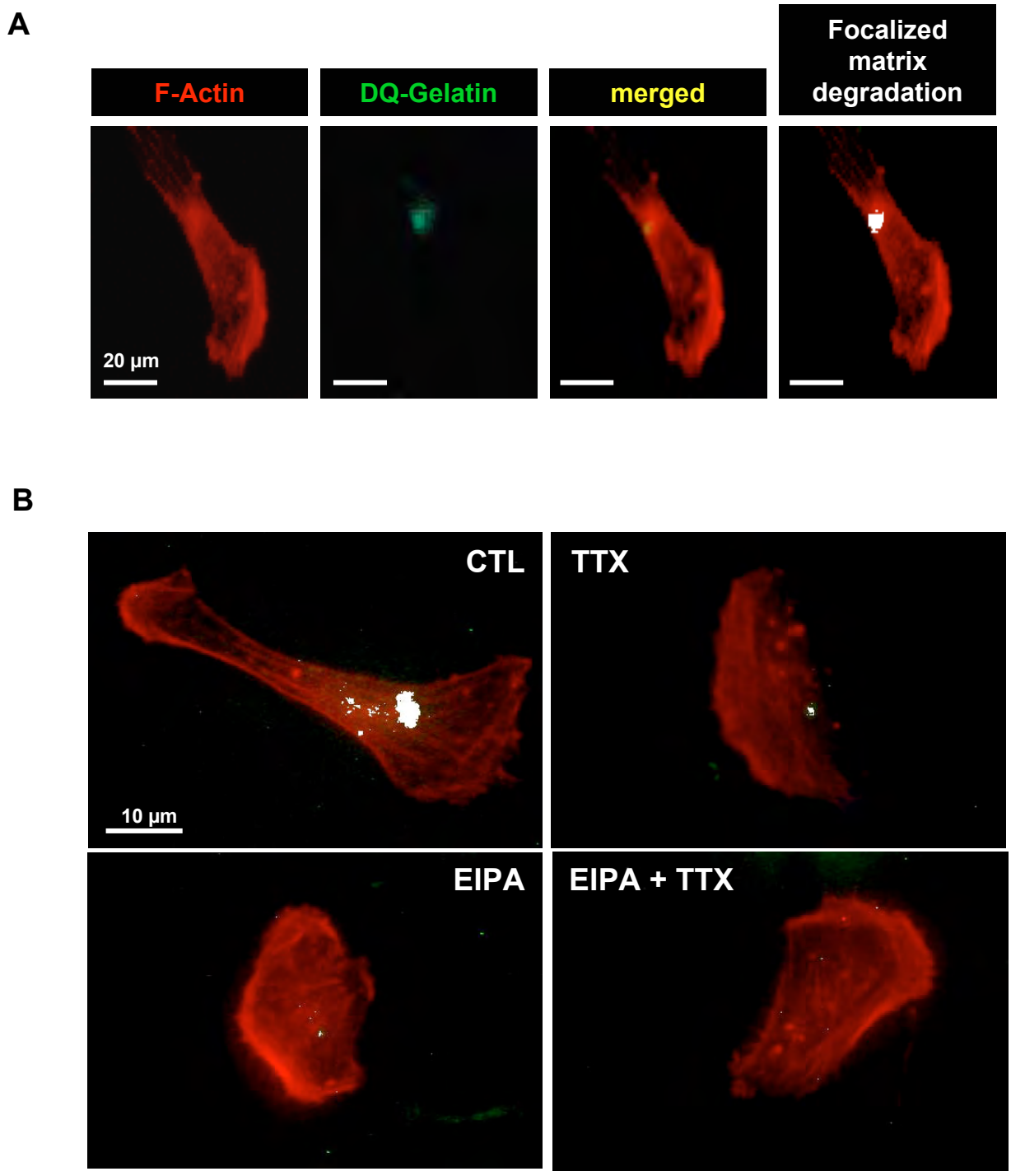

Fig. S4: A, The invadopodial activity in MDA-MB-231 cancer cells cultured on a Matrigel™-composed matrix containing DQ-Gelatin® was assessed and defined as being F-actin foci (red labelling, phalloidin-Alexa594) co-localised with focused proteolytic activities (green). Merging areas are represented as white pixels which are counted for every cell in order to calculate a "Matrix-Focalized-degradation activity index". **B**, representative pictures of MDA-MB-231 cells untreated (CTL) or treated with 30 µM TTX or 1 µM EIPA or a combination of TTX + EIPA. Matrix degradation areas merging with F-actin foci appear as white pixels which were counted. Numbers of white pixels by cell in the different treatment conditions were measured then normalized to the number obtained in CTL condition.

References

Gillet, L., Roger, S., Besson, P., Lecaille, F., Gore, J., Bougnoux, P., Lalmanach, G. and Le Guennec, J. Y. (2009). Voltage-gated Sodium Channel Activity Promotes Cysteine Cathepsin-dependent Invasiveness and Colony Growth of Human Cancer Cells. *J Biol Chem* 284, 8680-91.

Jezequel, P., Campone, M., Gouraud, W., Guerin-Charbonnel, C., Leux, C., Ricolleau, G. and Campion, L. (2012). bc-GenExMiner: an easy-to-use online platform for gene prognostic analyses in breast cancer. *Breast Cancer Res Treat* 131, 765-75.